

Water Vapor Effects on Corrosion of Fe–Cr and Fe–Cr–Ni Alloys Containing Silicon in CO₂ Gas at 818 °C

Thuan Dinh Nguyen · Jianqiang Zhang · David J. Young

Received: 18 November 2014 / Revised: 28 January 2015 / Published online: 7 February 2015
© Springer Science+Business Media New York 2015

Abstract Model alloys Fe–20Cr and Fe–20Cr–20Ni, with and without Si additions (0.1, 0.2 and 0.5 wt%), were exposed to Ar–20CO₂–20H₂O gas at 818 °C. All undoped alloys underwent breakaway corrosion, resulting in iron-rich oxide scales and internal carbide precipitates. Silicon addition significantly improved both oxidation and carburization resistance in wet CO₂, by forming a layer of silica beneath the chromia scale. Silicon-bearing austenitic alloys underwent scale spallation on cooling from reaction. The contributions of thermal and growth stresses to spallation, and of growth stresses to the onset of breakaway are discussed.

Keywords Alloy · Silicon · Water vapor · High temperature corrosion

Introduction

Oxyfuel combustion technology is being developed and tested for coal-fired power plants to reduce CO₂ emission. During this process, a mixture of pure oxygen and recirculated flue gas is used for combustion of coal. As a result, a flue gas consisting mainly of CO₂ and water vapor is generated, offering a simplified solution for separation, storage and disposal/reuse of CO₂. Stainless steels are commonly used in heat exchangers because of their good mechanical properties and corrosion

T. D. Nguyen · J. Zhang · D. J. Young (✉)
School of Materials Science and Engineering, University of New South Wales, Sydney, NSW 2052,
Australia
e-mail: d.young@unsw.edu.au

T. D. Nguyen
e-mail: thuan.nguyen@unsw.edu.au

J. Zhang
e-mail: j.q.zhang@unsw.edu.au

resistance. These steels usually form a protective chromia scale which is slow-growing in air/oxygen. However, it is found that the good corrosion resistance of stainless steels is degraded quickly in gas mixtures containing both CO₂ and water vapour [1–6].

The benefits of silicon addition on corrosion resistance of chromium-containing steels have been studied in dry CO₂ [7] and water vapour [8, 9] at different temperatures. Improved performance was found to be due to the formation of an additional protective SiO₂ layer. Earlier CO₂ studies [7] concerned model Fe–9Cr, Fe–20Cr and Fe–20Cr–20Ni, with and without Si additions. It is known that water vapour accelerates high temperature corrosion by CO₂. It is therefore important to determine whether the benefit provided by Si is available in H₂O–CO₂ gas, which is more relevant to the flue gas in oxyfuel combustion. In the case of Fe–9Cr, the acceleration in scaling caused by H₂O is so large as to overwhelm any silicon effect. The aims of the present paper were to compare corrosion of Fe–20Cr and Fe–20Cr–20Ni containing (0.1, 0.2, 0.5) % Si at 818 °C in wet and dry CO₂, and determine any beneficial effects of Si additions in the wet CO₂ gas corrosion.

Materials and Experiments

Eight model alloys Fe–20Cr and Fe–20Cr–20Ni with and without (0.1, 0.2, 0.5) wt% Si were prepared by arc melting pure metals Fe (99.97 %), Cr (99.995 %), Ni (99.95 %) and Si (98.5 %) under a protective Ar–5 %H₂ gas atmosphere, using a non-consumable electrode. A master alloy Fe–4.71Si was used to prepare very dilute Si alloys of the desired alloy composition. The composition of the master alloy was established by chemical analysis (ASTM E350, part 46–52, 1999). The resulting buttons were annealed at 1,150 °C for 50 h in flowing Ar–5 %H₂ gas for homogenization. The alloy grain sizes after annealing were 2.6 ± 2 mm for 20Cr alloys and 2.4 ± 1.8 mm for 20Cr20Ni alloys. Rectangular alloy coupons with dimensions of (1.3 ± 0.3) mm \times (6.5 ± 1) mm \times (8.4 ± 1.6) mm were surface ground to a 1,200-grit finish and ultrasonically cleaned in alcohol prior to reaction. Analysis by XRD confirmed that Fe–20Cr–(Si) alloys were ferritic and Fe–20Cr–20Ni–(Si) alloys austenitic.

All specimens were reacted at 818 °C in an Ar–20CO₂–20H₂O (volume%) mixture with a linear flow rate of 2 cm/s and a total pressure of 1 atm. The water vapour content of the reaction gas was confirmed by a precision dew-point meter (Michell, S8000). Weight changes of oxidized samples were measured using an analytic balance (Precisa 180A) with an accuracy of 0.1 mg. In weight gain kinetic plots shown here, each point represents a separate sample. Corrosion samples were characterized by X-ray diffractometry (XRD; PANalytical Xpert MPD) with Cu-K _{α} radiation, optical microscopy, scanning electron microscopy (SEM, acceleration voltage 15 kV; Hitachi S3400) with an energy dispersive X-ray spectrometer (EDX, Bruker) and transmission electron microscopy (TEM; Philips CM200). The etchant used to reveal carbides in reacted samples was a modified glyceric acid solution (10 ml Glycerine + 6 ml hydrochloric acid + 3 ml HNO₃) at room temperature.

Results

Corrosion of Fe–20Cr–(Si) Alloys

Weight gain kinetics for Fe–20Cr–(Si) alloys in dry and wet gases are shown in Fig. 1. The rate of weight gain of Fe–20Cr in wet gas was significantly faster than that in dry gas. However, weight uptakes of the Si-containing alloys in dry CO₂ [7] and wet CO₂ gas (Fig. 1) were markedly smaller than those of the undoped Fe–20Cr alloy. No apparent scale spallation was observed for any alloy in either gas.

In dry CO₂ gas, a uniform protective Cr₂O₃ scale was formed on Fe–20Cr [7]. However, in wet CO₂ gas, this alloy formed Cr₂O₃ scales (Fig. 2a, c) together with randomly distributed nodules consisting of an outer Fe₂O₃ layer, an intermediate (FeCr₂O₄ + Fe₃O₄) layer and an inner Cr₂O₃ layer (Fig. 2d). All three layers were identified in Ref. [10]. Blade-shaped whiskers were observed on chromia scales in the wet CO₂ reaction (Fig. 2b), but not in dry CO₂ [7].

Diffraction patterns from the surfaces of Fe–20Cr–0.5Si and Fe–20Cr–20Ni–0.5Si after reaction in wet CO₂ for 240 h in Fig. 3 show that thin Cr₂O₃ scales formed on the alloys. No other oxide phases were detected from these patterns.

Like the undoped Fe–20Cr alloy, Si-containing Fe–20Cr alloys also formed whiskers on the surface after reactions in wet CO₂ gas (Fig. 4). These whiskers had

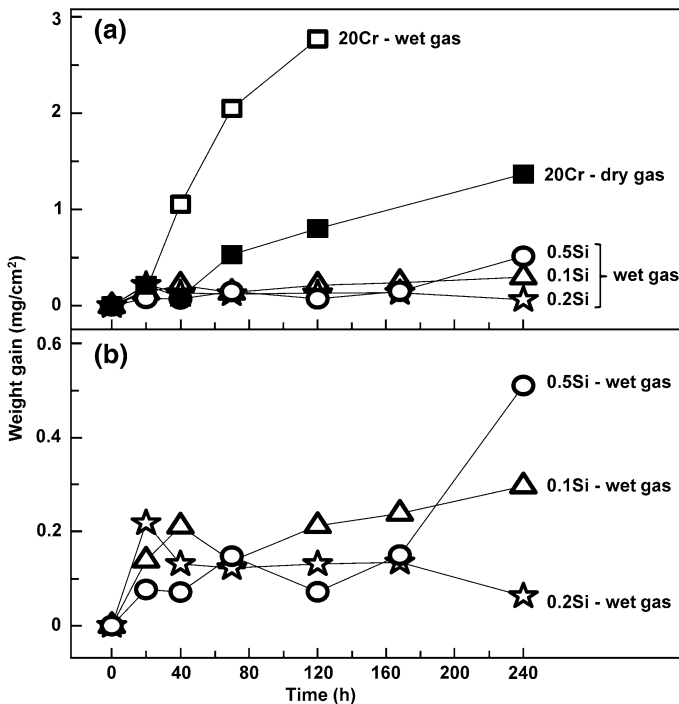


Fig. 1 a Weight gain kinetics of Fe–20Cr–(Si) alloys in Ar–20CO₂ and Ar–20CO₂–20H₂O. b An enlarged graph of Fe–20Cr–(0.1, 0.2, 0.5)Si in (a)

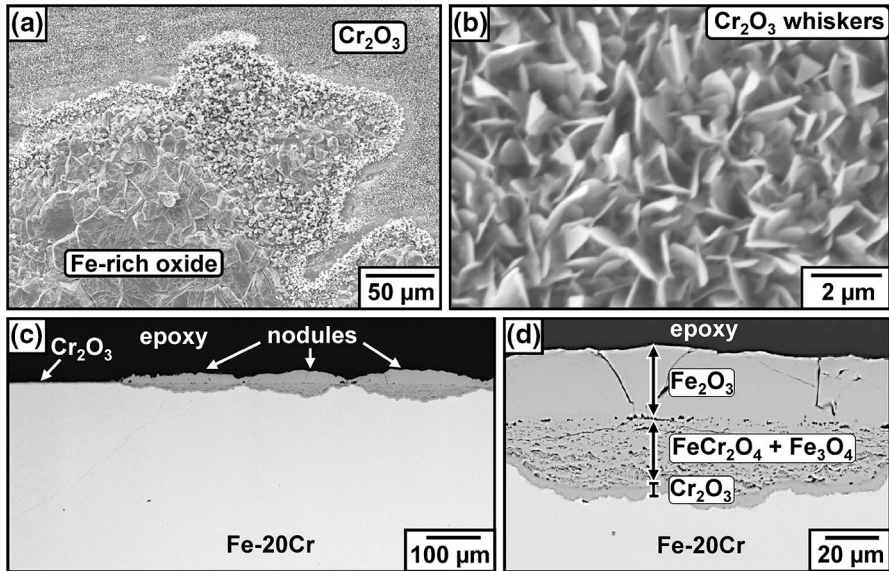


Fig. 2 Fe-20Cr after reaction in Ar-20CO₂-20H₂O for 70 h. **a** SE-SEM top-view, **b** high magnification image of Cr₂O₃ region in (a). **c** BSE-SEM cross-section, and **d** BSE-SEM high magnification image of oxide nodules in (c)

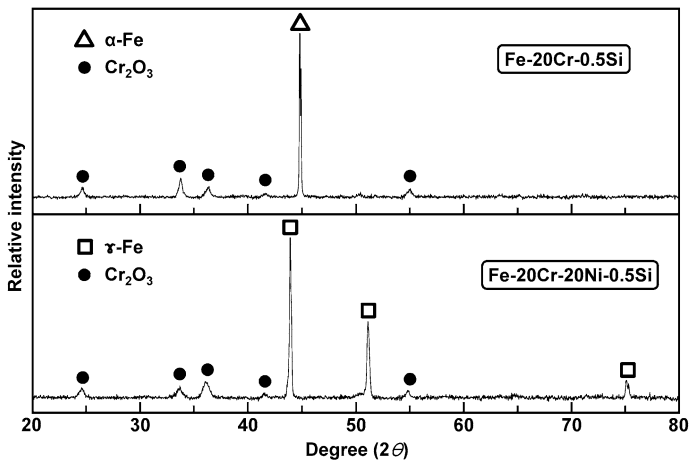


Fig. 3 XRD patterns of Fe-20Cr-0.5Si and Fe-20Cr-20Ni-0.5Si after reaction for 240 h in Ar-20CO₂-20H₂O

a blade shape and grew in different directions. Beneath this whisker layer was a solid Cr₂O₃ layer (Fig. 5a). Analysis by EDX (Fig. 5b) shows that a Si-rich oxide layer also formed at the scale-alloy interface. Results of TEM and EDX (Fig. 5c, d)

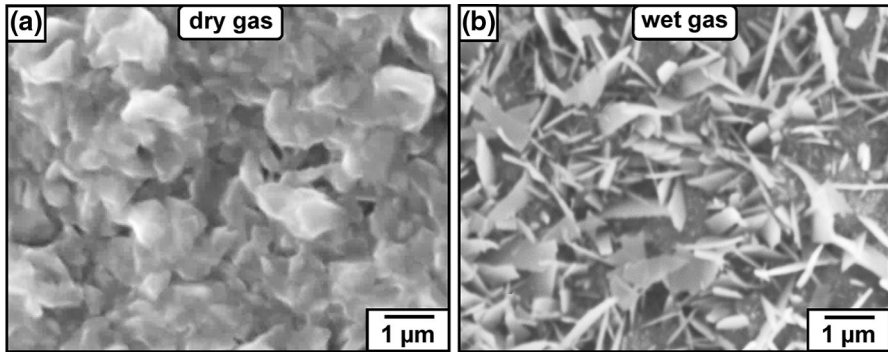


Fig. 4 SE-SEM top-views of Fe–20Cr–0.5Si after reaction in **a** Ar–20CO₂ (240 h) and **b** Ar–20CO₂–20H₂O (120 h)

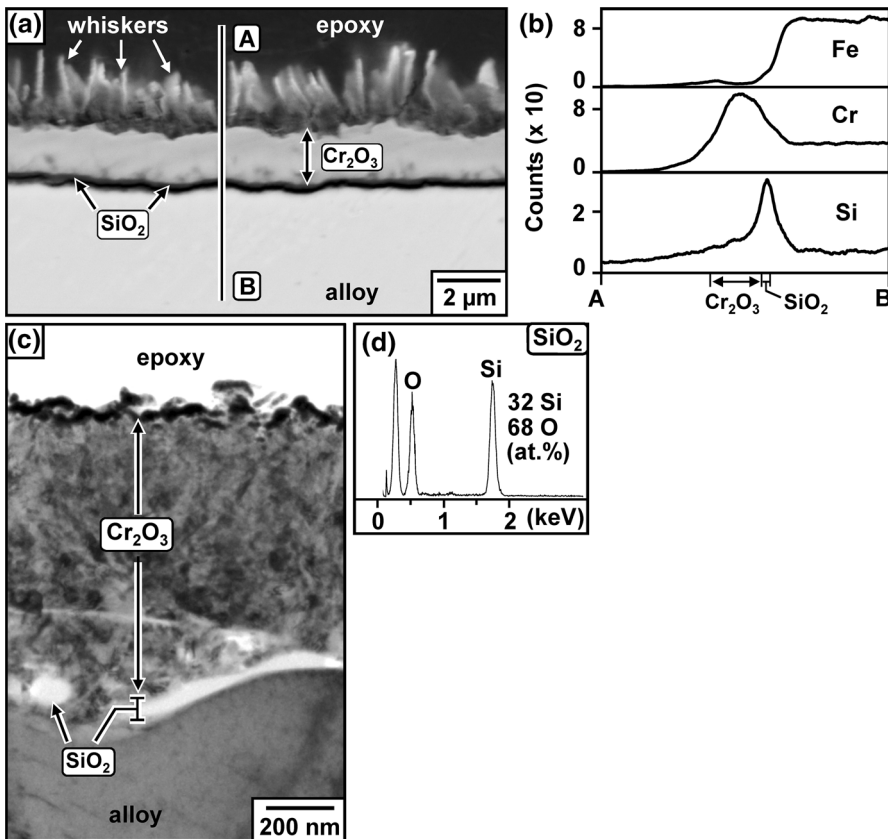


Fig. 5 Fe–20Cr–0.5Si in Ar–20CO₂–20H₂O after reaction for: **a** (120 h) BSE-SEM cross-section, **b** EDX line profiles along A–B shown in (a), **c** (240 h) Bright field TEM image and **d** EDX spectrum of SiO₂ layer in (c)

confirmed the Si-rich oxide layer to be SiO_2 . Similarly, Fe–20Cr–0.2Si formed an amorphous SiO_2 layer at the scale-alloy interface after reaction in dry CO_2 gas [7].

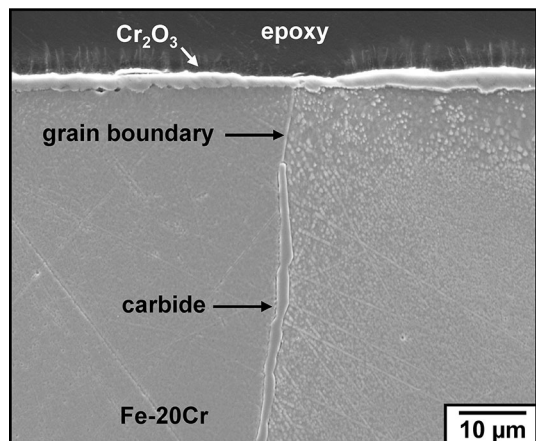
In wet CO_2 gas, the undoped Fe–20Cr alloy underwent not only oxidation but also carburization, resulting in the precipitation of internal carbides, as seen in Fig. 6. However, no carbide was found in any Si-containing Fe–20Cr alloys reacted with the wet gas. In dry CO_2 gas, the same difference was seen in carburization behaviour between Si-free and Si-bearing alloys [7].

Corrosion of Fe–20Cr–20Ni–(Si) Alloys

Weight uptake kinetics of Fe–20Cr–20Ni–(Si) in dry and wet gases are shown in Fig. 7. The weight gains of the undoped Fe–20Cr–20Ni alloy were substantial in both gases. In each case, an initial period of slow reaction was followed by a much faster reaction, the onset of rapid corrosion occurring sooner in wet gas. The kinetics of the wet gas reaction appear parabolic with time. In contrast, additions of (0.1, 0.2) % Si led to dramatically lower weight gains in wet CO_2 . The weight gains of Fe–20Cr–20Ni–0.5Si after reactions for 70, 120 and 168 h in wet CO_2 were slightly higher than those of Fe–20Cr–20Ni–(0.1, 0.2)Si. Scale spallation occurred occasionally for all alloys during cooling in wet CO_2 gas, and the reported weight gains are therefore underestimated.

Weight uptakes by Fe–20Cr–20Ni were higher than those of the Si-containing alloys because of the formation of iron-rich oxide nodules, as seen in Fig. 8. After 40 h reaction in wet CO_2 , regions of protective Cr_2O_3 scale on this alloy (Fig. 8a) were interrupted by iron-rich oxide nodules, which were identified as Fe_2O_3 by XRD analysis. Whiskers also formed on the outermost surface of the Cr_2O_3 scale (Fig. 8b). An alloy deformation zone containing fine grains with different sizes was observed beneath the Cr_2O_3 scale (Fig. 8c). This zone was formed as a result of cold working the alloy surface during specimen preparation. Analysis by EDX (Fig. 8d) showed that the deformation zone was the main Cr supply for scale growth. After a

Fig. 6 Carbide in Fe–20Cr (etched) after reaction for 70 h in Ar–20 CO_2 –20 H_2O



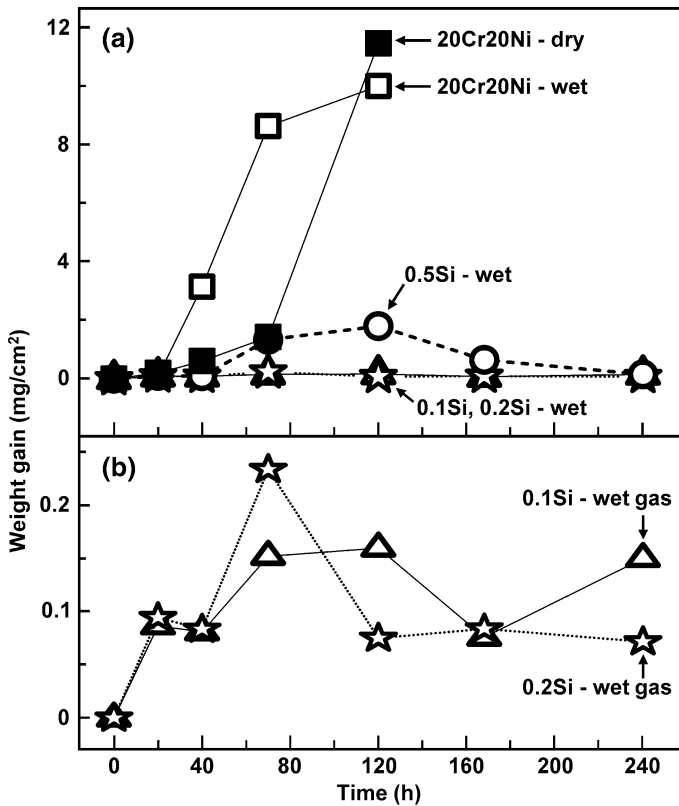


Fig. 7 a Weight gain kinetics of Fe–20Cr–20Ni–(Si) alloys in Ar–20CO₂ and Ar–20CO₂–20H₂O. b An enlarged graph of Fe–20Cr–20Ni–(0.1, 0.2)Si in (a)

longer reaction time of 70 h in wet CO₂, this undoped alloy had formed a uniform iron-rich oxide scale [10].

Unlike the chromia scales on Fe–20Cr–20Ni, those on the Si-containing austenitic alloys remained protective for longer, as seen in Fig. 9. After 240 h reaction in dry CO₂, the chromia scale on Fe–20Cr–20Ni–0.1Si (not shown) and Fe–20Cr–20Ni–(0.2, 0.5)Si (Fig. 9a, b) consisted of very fine oxide grains without any scale spallation. However, when these alloys reacted in wet CO₂ gas, whiskers formed on chromia scale surfaces, and spallation was observed on cooling (Fig. 9c, d). The Si-free Fe–20Cr–20Ni alloy also spalled during cooling. However, after short reaction times, the thin chromia scale regions did not spall, whereas some of the Fe-rich oxide became detached.

Detachment of scale fragments left areas of bare metal surface. Scratches on the sample surface resulting from grinding prior to reaction were still observed on scale-free areas (Figs. 9d, 10) and on the adjacent chromia scales (Fig. 9d). The scale-free areas (Fig. 10) are seen to be smooth, containing fine voids along grain boundaries. Compositions of these spalled areas found by EDX analysis (not shown) are rich in

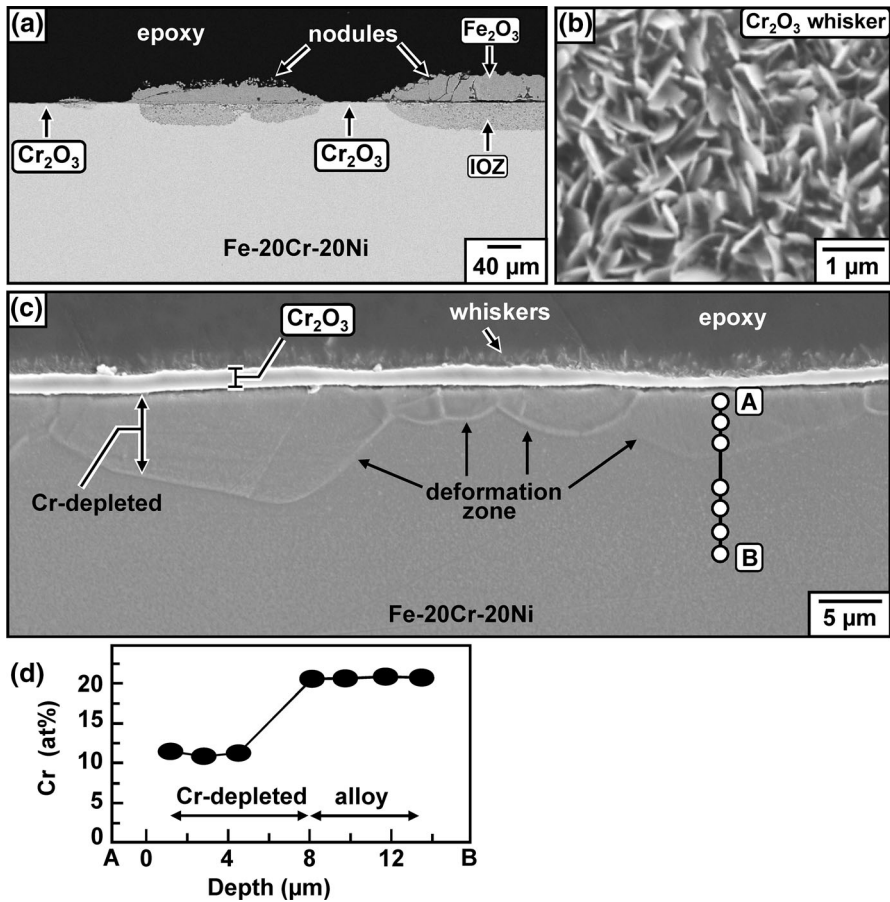


Fig. 8 Fe-20Cr-20Ni after reaction in Ar-20CO₂-20H₂O for 40 h: **a** BSE-SEM cross-section, **b** SE-SEM top-view of thin Cr₂O₃ scale, **c** high magnification image of Cr₂O₃ region in (a), and **d** EDX analysis along A-B beneath the scale shown in (c)

Fe and Ni. Clearly, scale spallation on these Fe-rich areas happened only during cooling, leaving clean, unreacted metal.

In dry CO₂ gas [7], no iron oxide nodules were formed on any Si-containing austenitic alloys. However, in wet CO₂ gas, iron oxide nodules were observed on Fe-20Cr-20Ni (Fig. 8), also on Fe-20Cr-20Ni-0.5Si (Fig. 11), but not on Fe-20Cr-20Ni-(0.1, 0.2)Si.

After 70 h reaction in wet CO₂, Fe-20Cr-20Ni-0.5Si formed a thin scale together with randomly distributed nodules (Fig. 11a). The thin scale (Fig. 11b) consisted of an outer continuous Cr₂O₃ layer and an inner discontinuous Si-rich oxide layer as identified in Fig. 11c. Analysis by TEM/EDX (not shown) confirmed the Si-rich oxide layer to be SiO₂.

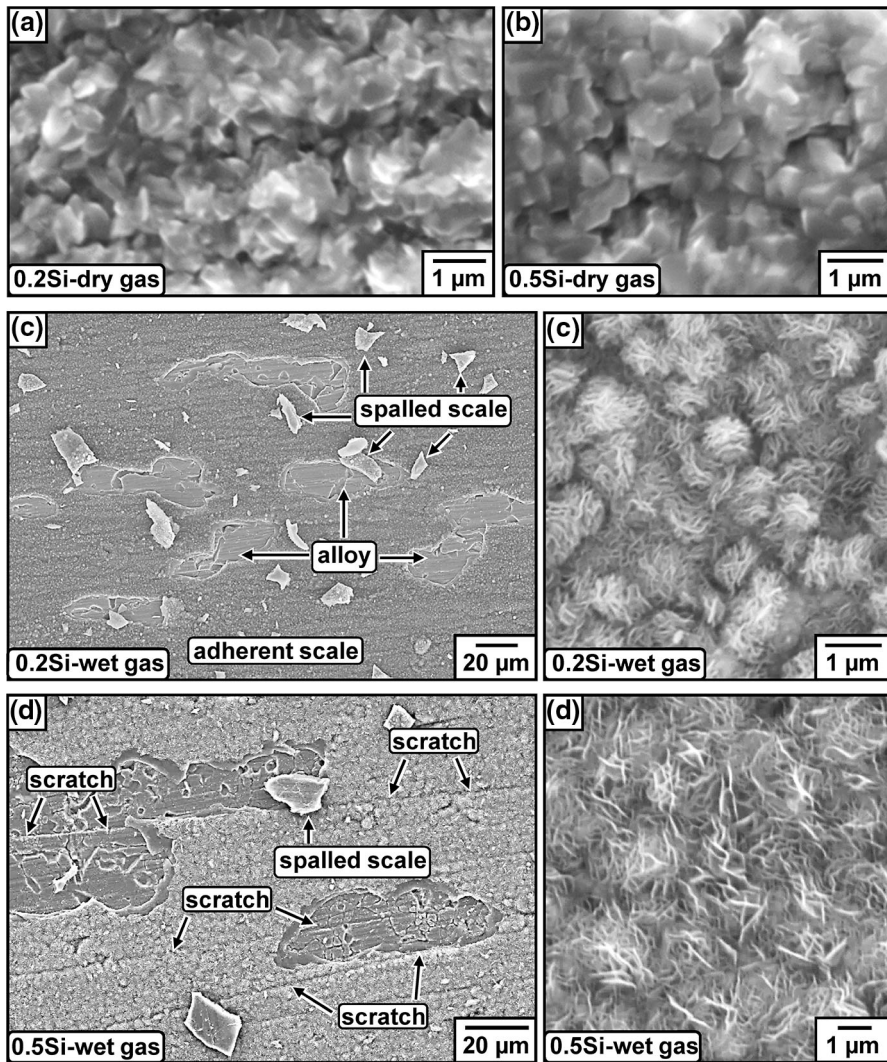


Fig. 9 SE-SEM *top* views of **a** Fe–20Cr–20Ni–0.2Si and **b** Fe–20Cr–20Ni–0.5Si reacted in Ar–20CO₂ (240 h). SE-SEM *top* views (*left*) and high magnification images (*right*) of thin scales on **c** Fe–20Cr–20Ni–0.2Si and **d** Fe–20Cr–20Ni–0.5Si reacted in Ar–20CO₂–20H₂O (240 h)

Reaction in dry [7] and wet CO₂ gases resulted in both oxidation and carburization for the undoped Fe–20Cr–20Ni alloy, as shown in Fig. 12 for the wet case. Carbides were observed in this alloy after reaction in wet CO₂ for 70 h. In contrast, metallographic examination confirmed that no carbides were formed in any Si-containing Fe–20Cr–20Ni alloy in either dry [7] or wet CO₂ gases.

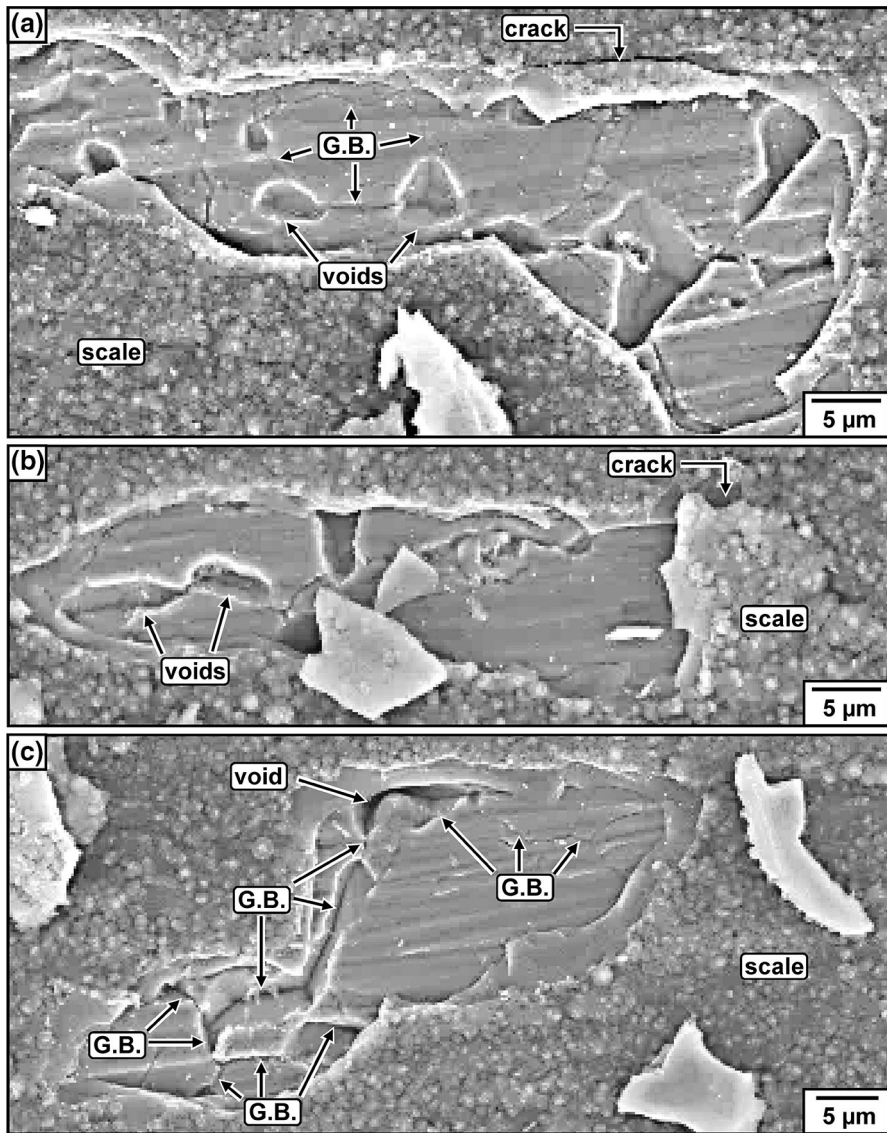


Fig. 10 Enlarged images of scale-free areas of Fe-20Cr-0Ni-0.2Si in Fig. 9c, showing voids along grain boundaries (G. B.)

Discussion

Effects of Si on Carburization in Dry and Wet CO₂

Alloys exposed to dry and wet CO₂ gases may undergo carburization and/or oxidation. Carbides were observed in the undoped alloys after reactions in both dry

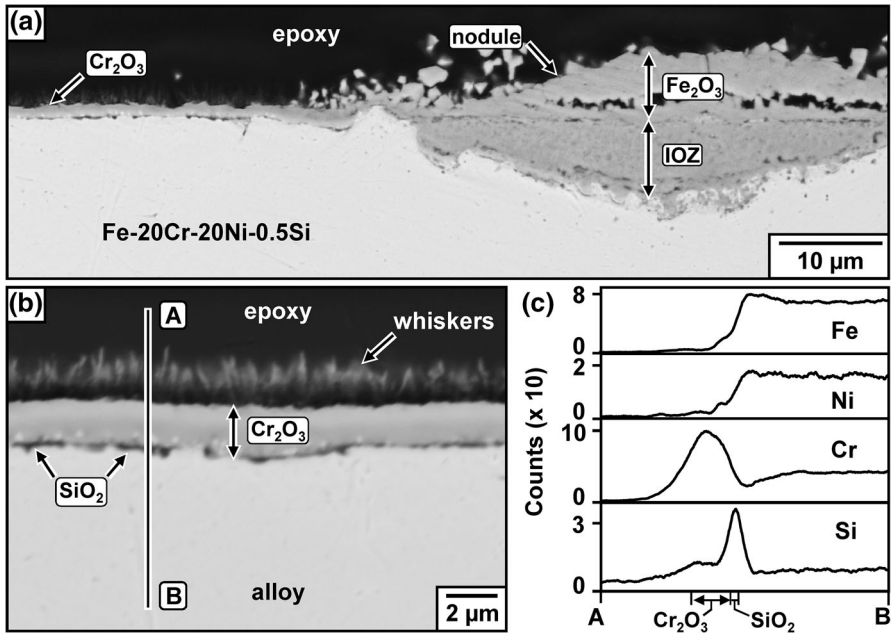
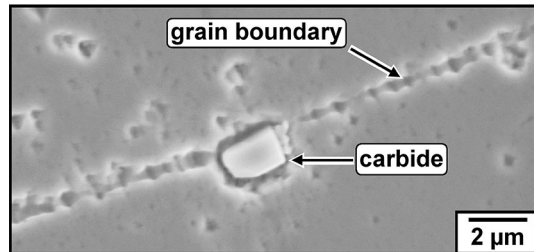


Fig. 11 a BSE-SEM cross-section of Fe-20Cr-20Ni-0.5Si after reaction in Ar-20CO₂-20H₂O for 70 h, b BSE-SEM high magnification image of thin Cr₂O₃ scale in (a) and c EDX analysis along A-B shown in (b)

Fig. 12 Carbide in Fe-20Cr-20Ni (etched) after reaction for 70 h in Ar-20CO₂-20H₂O



and wet CO₂ gases, but not the Si-bearing alloys. Thus silicon additions were very effective in preventing carburization.

Oxidation and carburization happen simultaneously during reaction in dry and wet CO₂ due to the transfer of oxygen and carbon from the reaction gas to the alloys by reactions:





At first sight, it appears that equilibrium carbon activities in the gas phase ($a_{\text{C}} = 1 \times 10^{-13}$ in Ar-20CO₂ at 818 °C) are too low for alloy carburization. Nevertheless, the maximum carbon activity *at the scale-alloy interface* calculated from (1) and (2), using standard thermodynamic data and an oxygen partial pressure set by the iron oxide scale-alloy interfacial equilibrium has been found to be large enough for carburization to occur [4, 11].

Thermocalc-computed phase diagrams [12] (Fig. 13) show that adding Si to Fe-20Cr and Fe-20Cr-20Ni has very little effect on the critical carbon activities required to form carbides. It is therefore concluded that the effect of Si in preventing

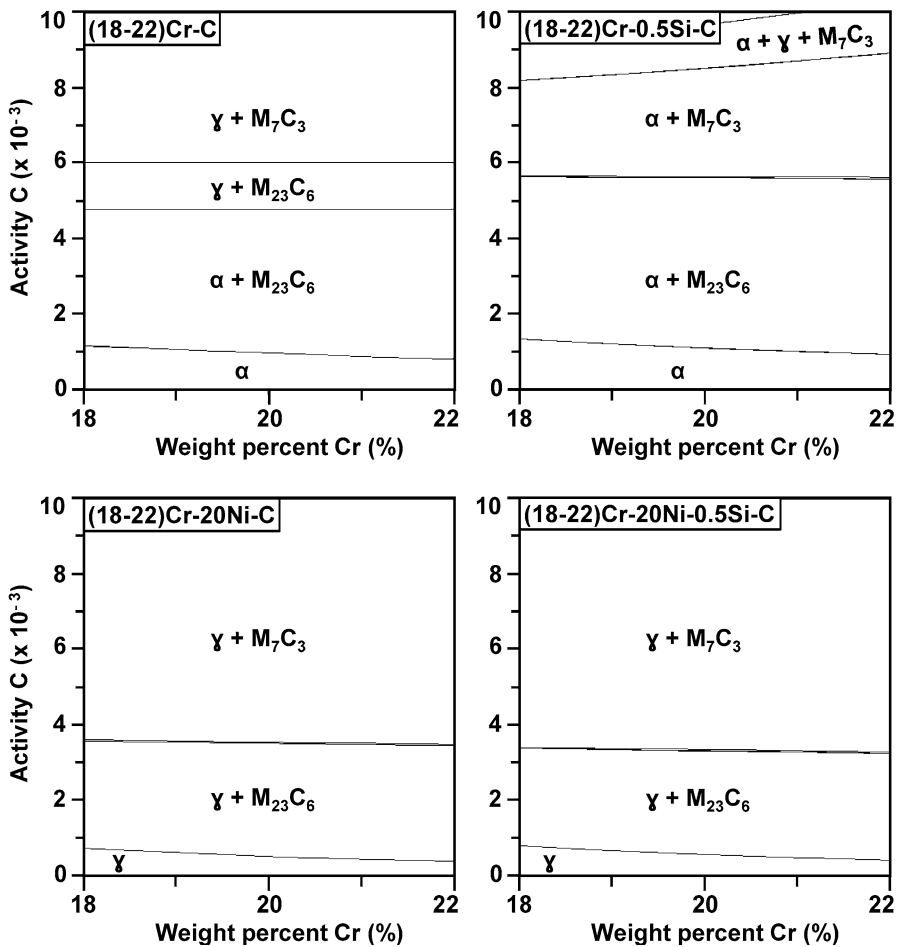


Fig. 13 Isothermal sections (Thermo-Calc [12]) of Fe-20Cr-(0.5Si)-C and Fe-20Cr-20Ni-(0.5Si)-C at 818 °C

carbide formation is not due to thermodynamic interaction with carbon in ferrite or austenite.

Chromia scales are usually considered to be a good diffusion barrier for oxidation resistance because of their high density and slow growth. It was discovered recently [13], however, that carbon is able to penetrate protective chromia scales via oxide grain boundaries, enabling carburization of the underlying alloy. For this reason, carbides were observed in Si-free alloys beneath their otherwise protective chromia scales after reactions in dry [7] and wet CO₂ (Fig. 6). It is concluded that a single layer of iron oxide or chromia on the surface of Cr-containing alloys is not enough to effectively prevent carbon penetration from the dry and wet CO₂ gases at high temperatures. A detailed discussion of water vapour effects on carburization of Fe–20Cr and Fe–20Cr–20Ni is available elsewhere [10].

Addition of Si to Fe–20Cr and Fe–20Cr–20Ni resulted in the formation of an additional silicon oxide layer beneath the chromia layer during reaction in dry [7] and wet CO₂ (Figs. 5, 11). The effectiveness of silicon oxide in preventing carburization has long been known [14]. Silica coatings deposited by a plasma-assisted vapour deposition method completely prevented carburization of Incoloy 800H (Fe–20Cr–31Ni) during reaction in H₂–4CH₄ ($a_C = 0.82$) at 825 °C [15]. Formation of a duplex scale of chromia and silica by heat resisting steels (with 1.8 wt% Si) exposed to steam-hydrocarbon mixtures also blocks carbon entry in the substrate [16]. It is concluded, therefore, that the same mechanism is operative in the wet CO₂ reaction: the presence of an additional protective silicon oxide layer beneath an outermost chromia layer effectively blocked carbon permeation at 818 °C in dry and wet CO₂ corrosion.

Effects of Si on Oxidation of Fe–20Cr in Dry and Wet CO₂

The good oxidation resistance of Fe–20Cr in dry CO₂ gas diminished greatly when exposed to wet CO₂ gas, whereas Fe–20Cr–(0.1, 0.2, 0.5)Si alloys demonstrated protective behaviour in both gases.

Water vapour is reported to accelerate the growth rate of Cr₂O₃ scales on Fe–22Cr in Ar–30H₂O–3O₂ at 650 °C [17] and on Fe–20Cr–25Ni in Air–10H₂O at 800 °C [18]. When an oxidizing atmosphere contains both water vapour and sufficient free oxygen, solid chromia may be converted to a volatile compound, CrO₂(OH)₂ [18]. However, the present experiments involve very low p_{O₂} values, and this mechanism is not applicable.

In this study, the oxidation resistance of the undoped Fe–20Cr alloy was found to change dramatically when water vapour was added to the reaction gas. Whereas, in dry CO₂, it formed a uniform protective Cr₂O₃ scale [7], in wet CO₂, it formed Cr₂O₃ plus iron rich oxide nodules (Fig. 2). The breakaway of protective chromia scales in wet gas may, in principle, be caused by insufficient Cr supply from the underlying alloy to sustain the accelerated chromia growth and/or mechanical stress resulting in failure of the scale.

The growth rate of chromia scales on Fe–20Cr and Cr depletion in the underlying alloy were found to be similar in dry and wet gases [10]. Therefore, severe Cr

depletion cannot be the main factor resulting in the breakaway of chromia scales grown in the wet CO₂ reaction [10].

Reactions in wet CO₂ led also to the formation of Cr₂O₃ whiskers on top of the solid chromia layer (Fig. 2b). Similarly, whiskers formed on pure chromium exposed to a H₂–1.5H₂O mixture at 900 °C [19]. Whiskers such as these produced in wet gas reactions have been proposed to grow primarily by surface diffusion of cations along an internal tunnel formed by a screw dislocation or a bundle of dislocations [20]. As these whiskers had non-parallel growth directions, they could contact and then push/press against each other during their growth, leading to higher stress at their roots within the solid chromia layer [10]. On this basis, the breakaway of Cr₂O₃ in the wet CO₂ gas reaction is suggested to be caused by the stresses developing during whisker growth [10].

It is concluded that 20 % Cr was sufficient to form and maintain a protective Cr₂O₃ scale in the dry CO₂ reaction, but failed to do so in the wet CO₂ reaction, which was a more complex process.

All of the Fe–20Cr–(0.1, 0.2, 0.5)Si alloys were protective in both dry [7] and wet CO₂ (Figs. 1, 5). A slow-growing silicon oxide layer at the chromia-alloy interface in dry [7] and wet CO₂ (Fig. 5) provided an additional diffusion barrier. As already reported [7], the chromia scales on Si-containing alloys are thinner than that on the undoped Fe–20Cr alloy in the dry CO₂ reaction [7]. Similarly, after reaction for 120 h in wet CO₂, the solid chromia scale on Fe–20Cr–0.5Si (1.5 μm thick) (Fig. 5) was thinner than that on Fe–20Cr (3.4 μm thick) [10]. It is concluded, therefore, in agreement with earlier workers [21, 22] that the additional silicon oxide layer at the chromia-alloy interface reduced the growth rate of the overlying solid chromia layer in both dry and wet CO₂, by slowing outward chromium diffusion.

Effects of Si on Oxidation of Fe–20Cr–20Ni in Dry and Wet CO₂

The undoped Fe–20Cr–20Ni alloy underwent breakaway oxidation in dry [7] and wet CO₂ (Fig. 8), but the additions of Si to this alloy markedly reduced the oxygen uptake in both dry CO₂ [7] and wet CO₂ (Fig. 7).

At an early stage of oxidation, Fe–20Cr–20Ni formed chromia scales and iron rich oxide nodules in dry [7] and wet CO₂ (Fig. 8). An alloy deformation zone with small grains was observed beneath the chromia scale (Fig. 8c). Analysis by EDX along the line A-B in Fig. 8d showed that the deformation zone was depleted in chromium. The amount of Cr in the solid scale is evaluated assuming the scale to be pure Cr₂O₃

$$\frac{\Delta W_{Cr}^{Oxide}}{A} = \frac{2X\rho M_{Cr}}{M_{Cr_2O_3}}. \quad (4)$$

Here $\Delta W_{Cr}^{Cr_2O_3}/A$ is the amount of Cr in the scale per unit surface area, ρ the oxide density, M_i the molecular weight of the indicated species, and X the thickness of the solid chromia layer above the A-B line (about 1 μm), neglecting the whiskers layer

The amount of Cr removed from the Fe–20Cr–20Ni alloy during oxidation can be calculated directly from concentrations measured in the Cr depletion zone beneath the scale (Fig. 8d), assuming no Cr was consumed to form carbides and the density of the Cr depletion zone and the alloy to be the same.

$$\frac{\Delta W_{\text{Cr}}^{\text{Alloy}}}{A} = \int_0^Y (C^0 - C) dx. \quad (5)$$

Here $\Delta W_{\text{Cr}}^{\text{Alloy}}/A$ is the amount of Cr lost from the alloy, Y the total Cr depletion depth, C^0 the original and C the remaining alloy Cr concentration, expressed as mass per unit volume.

The value of $\Delta W_{\text{Cr}}^{\text{Oxide}}/A$ calculated using Eq. (4) for Fe–20Cr–20Ni after reaction for 40 h is $3.6 \times 10^{-4} \text{ g cm}^{-2}$, when X is evaluated at the point labelled A in Fig. 8c. This is to be compared with the measured alloy Cr depletion level using Eq. (5), $\Delta W_{\text{Cr}}^{\text{Alloy}}/A$, of $3.8 \times 10^{-4} \text{ g cm}^{-2}$, where Y is measured at the same place. The mismatch between amounts of chromium in the scale and depleted from the alloy is due to the presence of additional Cr_2O_3 whiskers on top of the solid Cr_2O_3 layer.

The deformation zone was shown by the mass balance to be the main Cr supply for the chromia growth. However, in longer reactions, this thin (3–10 μm thick) and nonuniform zone failed to receive enough Cr resupply from the underlying alloy, limited as it was by very slow volume diffusion. Consequently, severe Cr depletion in the deformation zone led to breakaway oxidation.

Prior use [10] of Wagner's theory [23] led to the predictions for austenitic Fe–20Cr–20Ni that the critical levels of N_{Cr} required to support exclusive Cr_2O_3 scale growth were 0.40 in dry CO_2 [10] and 0.42 in wet CO_2 [10]. Thus 20 % Cr was not enough to form and maintain the chromia scale in either gas. The chromia scale formed in the early stages was therefore replaced by a uniform iron oxide scale when reactions proceeded to longer times in both dry [7] and wet [10] gases.

The addition of a small amount of Si to Fe–20Cr–20Ni greatly reduced oxygen uptake in both dry [7] and wet (Fig. 7) CO_2 gases. A thin silicon oxide layer at the chromia-alloy interface (Fig. 11) served as an additional diffusion barrier together with the chromia layer. In dry CO_2 , all Si-containing alloys formed protective scales without any nodules [7]. In wet CO_2 , the austenitic alloys with low concentrations of (0.1, 0.2) % Si formed only a thin scale, but Fe–20Cr–20Ni–0.5Si formed a thin scale plus nodules (Fig. 11). It is concluded that Si additions from 0.1 to 0.5 % significantly improved oxidation resistance of Fe–20Cr–20Ni in dry and wet CO_2 reactions, by slowing chromia growth rates and lessening the need for high Cr supply capabilities. However, in wet CO_2 , the protective behaviour was affected by the level of Si. The Si-bearing austenitic alloys started to form iron-rich oxide nodules when the Si concentration increased to 0.5 %, as considered below.

Mechanical Effects

The onset of breakaway oxidation can be accelerated by local mechanical damage to the scale, allowing gas access to the underlying alloy and accelerated chromium depletion [24]. Even more extensive mechanical damage is evident in the scale spallation which occurred during cooling after reaction of certain alloys. This more obvious effect is considered first.

Scale Spallation

Spallation of the thin, protective scale was observed in the case of austenitic Fe–20Cr–20Ni–Si alloys, but not Fe–20Cr–20Ni, during cooling after reaction in wet gas. None of these alloys suffered spallation after reaction in dry gas. In contrast, the Fe–20Cr alloys, with and without Si additions, underwent no spallation after reaction in either wet or dry gas. In addition, no alloy sustained spallation damage during isothermal reaction in either wet or dry CO₂. Some understanding of this complex pattern of behaviour can be gained from a consideration of how the stresses causing spallation can arise.

For the total stress, σ_T , in the scale after cooling, one can write

$$\sigma_T = \sigma_{CTE} + \sigma_g, \quad (6)$$

with σ_{CTE} the stress resulting from cooling due to the difference between the metal and oxide coefficients of thermal expansion, and σ_g the stresses accumulated in the scale during its growth. For simplicity, it is assumed here that growth stresses are not relaxed during cooling. Clearly, the value of σ_g is less than the critical value for spallation, σ_{crit} , as no spallation occurred prior to cooling of any alloy after reaction in either gas.

One obvious difference between the two alloy groups is in the value of σ_{CTE} . Linear thermal expansion coefficients of ferritic steels (about $13.1 \times 10^{-6} \text{ K}^{-1}$) [25] are smaller than those of austenitic steels (about $19.5 \times 10^{-6} \text{ K}^{-1}$) [25]. It follows, therefore, that the thin scales on Si-containing austenitic Fe–Cr–Ni alloys developed higher σ_{CTE} values during cooling than did those on the Si-bearing ferritic alloys. Furthermore, σ_T (γ -alloy) $>$ σ_T (α -alloy) if σ_g is the same in each case. However, the outcome (spallation or not, upon cooling) obviously depended not only on σ_{CTE} , but also upon the reaction gas and whether or not Si was present in the γ -alloy. It must therefore be concluded that σ_g is not negligible, rather it is the sum of terms in Eq. (6) causing σ_T to exceed σ_{crit} in some cases.

Comparing austenitic and ferritic 20Cr alloys, the spallation of the former under some circumstances, and the resistance of the latter under all circumstances can be attributed to the difference in σ_{CTE} . Comparisons among the different austenitic alloy reactions require more detailed consideration of scale morphologies.

Water vapour promoted the formation of whiskers growing from the thin protective scales (Figs. 4, 9). The growth of these whiskers during reactions has been suggested to increase stress in the underlying solid chromia layers [10], degrading their mechanical stability. The presence of Si in the alloys led to the

development of silica at the scale-alloy interface. The volume change accompanying silicon oxidation at this mechanically constrained interface would also contribute to an increase in stress. In addition, the isolated silicon particles sometimes observed (Fig. 11) could provide stress concentration locations. At least conceptually, Eq. (6) can be expanded to read

$$\sigma_T = \sigma_{CTE} + \sigma_W + \sigma_{Si} + \sigma_{Cr}, \quad (7)$$

where σ_W , σ_{Si} , and σ_{Cr} are growth stresses resulting from whisker growth, silica formation and growth of chromia itself. The implied linear independence of the growth stress terms is an oversimplification, but this is not important to the qualitative argument.

The thin scale regions on Fe–20Cr–20Ni–(0.1, 0.2, 0.5)Si alloys after reactions in dry [7] and wet CO₂ (Figs. 5, 11) reactions contained the same corrosion products of chromia and silicon oxide. Solid chromia scales on these Si-bearing austenitic alloys were thin and almost the same thickness in dry (about 0.8–1.5 μm thick after 240 h) [7] and wet CO₂ (about 1.6 μm thick after 240 h). However, spallation of these thin scales on cooling happened only after reaction in wet CO₂ (Fig. 9). An increased stress in the solid chromia scales caused by the whiskers developed in wet CO₂ reaction is suggested to be one of factors causing this unexpected event. Whiskers also formed on chromia scales grown on ferritic alloys in wet CO₂, but these scales did not spall because σ_{CTE} for the ferritic alloys is significantly smaller.

Silicon effects on scale spallation from austenitic alloys are also important. Thin scale regions grown in wet CO₂ on Fe–20Cr–20Ni did not spall on cooling. Thus the combination of σ_{CTE} and growth stresses associated with whiskers (and with dense chromia) is insufficient to cause spallation in this case. In contrast, austenitic alloys containing 0.1–0.5 Si all suffered scale spallation during cooling. These same alloys did not spall when cooled after reaction in dry CO₂, which produced no whiskers but did cause silica formation. It is therefore concluded that all three factors are required to produce thin scale spallation: high σ_{CTE} resulting from an austenitic substrate, high growth stresses due to whisker development, and additional growth stresses caused by silica formation at the scale-alloy interface.

Austenitic alloys retained a subsurface deformation zone after reaction (Fig. 8), because lattice diffusion in these alloys is slow. Examination of alloy surfaces at sites revealed by scale spallation (Fig. 10) reveals cavities at locations where alloy grain boundaries intersect the surface. These indicate grain boundary diffusion of Cr to support chromia scale growth. Conversely, the continued presence of grinding marks on the surface reflects slow intragranular diffusion. Cavities represent local loss of scale-alloy contact, and presumably render the scale more susceptible to spallation. This is another difference between austenitic and ferritic alloys, the latter providing much faster lattice diffusion, and annealing out their subsurface zones during reaction.

The cavities appear not to be decisive. They are presumably generated in the same way during reaction of the austenitic alloys with dry CO₂, but scales grown in this gas do not spall on cooling.

Breakaway Corrosion

Breakaway occurs when these alloys cease to oxidize chromium selectively, allowing fast-growing, iron-rich oxides to form. Selective oxidation of chromium becomes impossible when alloy depletion becomes so severe that the necessary flux of the metal to the scale-alloy interface can no longer be maintained. The diffusion kinetics of this situation have been analysed by Wagner [23], by comparing diffusion fluxes of chromium in the scale and alloy. Application of this methodology to Fe–20Cr reacted in CO₂ [10] showed that an original chromium level of 0.11 in a ferritic Fe–Cr alloy is required to maintain Cr₂O₃ scale growth. The Fe–20Cr has more than enough chromium to satisfy this requirement, and its failure in wet CO₂ is not thereby explained.

In fact chromium levels beneath protective scales on Fe–20Cr prior to the onset of breakaway were measured [10] after reaction in wet CO₂ as ~ 14 % at the alloy-scale interface, confirming that steady-state depletion in the ferritic alloy is not severe. Ultimately, however, the Fe–20Cr alloy suffers breakaway corrosion in wet CO₂, a transition which cannot be predicted by Wagner's steady-state analysis. The onset of breakaway in wet gas was attributed [10] to the growth of chromia whiskers, and the additional stress term, σ_w .

As seen in the previous section on spallation, the various growth stresses in scales grown in wet gas on austenitic alloys are sufficient, when added to σ_{CTE} , to cause spallation. During isothermal oxidation, $\sigma_{CTE} = 0$, and spallation does not occur. However, the growth stresses are in effect, exacerbated in the case of wet gas reactions by the growth of chromia whiskers. It is suggested that these stresses are, in total, sufficient to cause local scale cracking, but not significant spallation. Any such cracks could be healed by rapid oxidation of more chromium. A series of such events would, however, lead to accelerated alloy chromium depletion, and eventual breakaway.

The thin scales grown on Fe–20Cr and Fe–20Cr–20Ni are morphologically very similar, and growth stresses within them are expected to be nearly the same. Thus local scale damage might also be expected in the scale grown on the ferritic alloy. However, rapid alloy diffusion supports protective chromia regrowth in the case of Fe–20Cr.

The effect of Si additions in preventing, or at least postponing, the onset of breakaway is of interest. As noted above, the presence of Si in austenitic alloys promotes spallation after cooling. Its effect in increasing growth stresses deduced from this observation would be operative at reaction temperature. An increased probability of local scale failure, consequent enhancement in Cr depletion, and eventual progression to breakaway would be predicted if this were the only effect. However, silica formed at the scale-alloy interface also has the effect of slowing chromia scale growth.

Whisker growth in wet CO₂ appears to be unaffected by the presence of silicon, and the mechanical effects of Si are therefore confined to those arising from silica formation and the diminution in dense chromia layer thickness. This layer was 1.5 μm thick on Fe–20Cr–0.5Si compared with 3.4 μm on Fe–20Cr after reaction for 120 h in wet CO₂. On the basis [26] that stress intensity increases with layer

thickness, it is concluded that the dense chromia layer on the Si-containing ferritic alloys developed less stress than the corresponding layer on Fe–20Cr. If, furthermore, the term σ_{cr} in Eq. (7) is significant compared to the other growth stresses, the propensity for scale cracking is on this basis predicted to be decreased. Thus silicon additions have two opposing effects on the scale integrity.

Increasing alloy silicon concentrations has slightly different effects in ferritic and austenitic alloys. In the case of Fe–20Cr, silicon additions at each level examined led to growth of an essentially continuous silica layer, and σ_{Si} is therefore not expected to differ significantly among the Si-bearing ferritics. In the case of Fe–20Cr–20Ni, however, the silica is present as distributed particles, the number of which increases with N_{Si} . If these act as stress raisers, then some negative consequences for scale integrity might be anticipated. It is possible that such an effect accounts for the fact that the Fe–20Cr–20Ni–0.5Si had nucleated Fe-rich nodules, whereas the 0.1 and 0.2 Si alloy variants maintained thin, protective scales of chromia plus silica.

Conclusions

Undoped Fe–20Cr and Fe–20Cr–20Ni alloys underwent breakaway oxidation in wet CO₂. The Fe–20Cr alloy was able to form and maintain a protective Cr₂O₃ scale in dry CO₂, but failed to do so in wet CO₂. Internal carburization occurred in all undoped alloys, beneath their oxide scales, in both dry and wet CO₂.

Silicon additions markedly improved the oxidation resistance of ferritic Fe–20Cr and austenitic Fe–20Cr–20Ni alloys in both gases. A silicon oxide layer at the chromia layer-alloy interface reduced the outward Cr diffusion, resulting in a thinner chromia scale, reduced growth stresses, and less severe Cr depletion.

Additions of (0.1, 0.2, 0.5) % Si to Fe–20Cr were beneficial in both dry and wet CO₂ reactions. Low level additions had the same benefit for Fe–20Cr–20Ni in both gases, but the addition of 0.5 % Si led to the formation of local iron-rich oxide nodules during reactions in wet CO₂.

This is thought to be caused by alterations to scale growth stresses, resulting in local scale failure during reaction. The duplex scale of chromia and silicon oxide effectively prevented all internal carburization.

Scale spallation on cooling after reaction occurred only when stresses due to differences in coefficients in thermal expansion, to whisker growth in wet gas, and to silica formation at the scale-alloy interface were all operative.

Acknowledgments Financial support from the Australian Research Council's Discovery Program is gratefully acknowledged.

References

1. J. P. Abellan, T. Olszewski, H. J. Penkalla, G. H. Meier, L. Singheiser and W. J. Quadackers, *Mater High Temp.* **26**, 63 (2009).

2. N. Mu, K. Y. Jung, N. M. Yanar, G. H. Meier, F. S. Pettit and G. R. Holcomb, *Oxid. Met.* **78**, 221 (2012).
3. S. Dryepondt, A. Rouaix-Vande Put and B. A. Pint, *Oxid. Met.* **79**, 627 (2013).
4. T. Gheno, D. Monceau, J. Zhang and D. J. Young, *Corros. Sci.* **53**, 2767 (2011).
5. T. Gheno, D. Monceau and D. J. Young, *Corros. Sci.* **64**, 222 (2012).
6. T. Gheno, D. Monceau and D. J. Young, *Corros. Sci.* **77**, 246 (2013).
7. T. D. Nguyen, J. Zhang and D. J. Young, *Oxid. Met.* **81**, 549 (2014).
8. M. Schütze, D. Renusch and M. Schorr, *Corros. Eng. Sci. Technol.* **39**, 157 (2004).
9. G. H. Meier, K. Jung, N. Mu, N. M. Yanar, F. S. Pettit, J. P. Abellán, T. Olszewski, L. N. Hierro, W. J. Quadackers and G. R. Holcomb, *Oxid. Met.* **74**, 319 (2010).
10. T. D. Nguyen, J. Zhang and D. J. Young, *Corros. Sci.* **89**, 220 (2014).
11. T. D. Nguyen, J. Zhang and D. J. Young, *Scr. Mater.* **69**, 9 (2013).
12. Thermo-Calc Windows TCW2, version 2.2.1.1, 2003, FEDAT database.
13. D. J. Young, T. D. Nguyen, P. Felfer, J. Zhang and J. M. Cairney, *Scr. Mater.* **77**, 29 (2014).
14. R. H. Kane, *Corrosion* **37**, 187 (1981).
15. E. Lang, M. J. Bennett and C. F. Knights, *Mater. Sci. Eng.* **88**, 37 (1987).
16. D. J. Young, *High Temperature Oxidation and Corrosion of Metals*, 1st ed, (Elsevier, UK, 2008).
17. N. Mu, K. Y. Jung, N. M. Yanar, F. S. Pettit, G. R. Holcomb, B. H. Howard and G. H. Meier, *Oxid. Met.* **79**, 461 (2013) .
18. D. J. Young and B. A. Pint, *Oxid. Met.* **66**, 137 (2006).
19. E. A. Polman, T. Fransen and P. J. Gellings, *Oxid. Met.* **32**, 433 (1989).
20. G. M. Raynaud and R. A. Rapp, *Oxid. Met.* **21**, 89 (1984).
21. H. E. Evans, D. A. Hilton, R. A. Holm and S. J. Webster, *Oxid. Met.* **19**, 1 (1983).
22. M. J. Bennett, M. R. Houlton and R. W. M. Hawes, *Corros. Sci.* **22**, 111 (1982).
23. C. Wagner, *J. Electrochem. Soc.* **99**, 369 (1952).
24. G. C. Wood and D. P. Whittle, *Corros. Sci.* **7**, 763 (1967).
25. F. Cervera, *ASM Ready Reference: Thermal Properties of Metals*, 1st ed, (ASM International, Materials park, 2002).
26. S. Daghigh, J. L. Lebrun and A. M. Huntz, *Mater. Sci. Forum* **251–254**, 381 (1997).